Heterometal Clusters Containing the Cuboidal Fe_4S_3 Fragment: Synthesis, Electron Distribution, and Reactions

Wei Cen, Frederick M. MacDonnell,[1] Michael J. Scott, and R. H. Holm*

Department of Chemistry, Harvard University, Cambridge, Massachusetts 02138

Received April 7, 1994[⊗]

The heterometal clusters $MFe_4S_6(PEt_3)_4Cl$ [M = V (**1**), Mo (**2**)] contain a cuboidal Fe_4S_3 fragment that is bridged by three μ_2-S atoms to the heterometal, forming a MFe_4S_6 core structure of idealized C_{3v} symmetry. Three symmetry-related (equatorial) Fe atoms and the M atom have terminal phosphine ligands while the unique (axial) Fe atom is terminally coordinated by chloride. These clusters and others prepared in this work are of primary interest because their $Fe_4(\mu_3\text{-}S)_3(\mu_2\text{-}S)_3$ portion structurally resembles a corresponding portion of the core of the FeMo-cofactor cluster of nitrogenase established by protein crystallography. Improved preparations of **1** and **2** are reported. Reaction of these clusters with NaSR in acetonitrile/THF yielded $VFe_4S_6(PEt_3)_4(SR)$ [R = Ph (**3**), Et (**5**)] and $MoFe_4S_6(PEt_3)_4(SR)$ [R = Ph (**4**), Et (**6**)]. Compound **3** crystallizes in triclinic space group $P\bar{1}$ with a = 12.094(3) Å, b = 13.651(3) Å, c = 16.840(6) Å, α = 112.19(2)°, β = 91.30(2)°, γ = 114.70(2)°, and Z = 2. Compound **4** crystallizes in monoclinic space group $P2_1/n$ with a = 20.796(6) Å, b = 19.006(4) Å, c = 26.076(7) Å, β = 108.64(2)°, and Z = 8. Both compounds exhibit the core structure of **1** and **2**; thiolate is bound at the axial site to form tetrahedral $FeS_3(SR)$ units. Molybdenum clusters **2** and **4** exhibit dimensionally expanded cuboidal fragments compared to vanadium clusters **1** and **3**. Collective structural and Mössbauer and ^{1}H NMR spectroscopic results indicate that the additional valence electron in the molybdenum clusters is largely delocalized in the Fe_4S_3 cuboidal portion. Cluster **1** exhibits the first example of a spin state equilibrium ($S = 0 \rightleftarrows S = 1$) in any iron–sulfur cluster. Clusters **2** and **4** have $S = {}^1/_2$ or spin-admixed ($S = {}^1/_2, {}^3/_2$) ground states. All clusters are readily identified by their characteristic ^{1}H NMR spectra, in which the axial thiolate substituents exhibit contact shifts indicative of negative spin delocalization.

Introduction

The heterometal cubane-type clusters containing the $[MFe_3(\mu_3\text{-}S)_4]$ core of idealized C_{3v} symmetry have played a central role in the development of biologically related metal–sulfur cluster chemistry.[2-7] The coordination units of the M = V and Mo clusters continue to be the closest synthetic approaches to the coordination environments of vanadium and molybdenum in their respective nitrogenase cofactors.[8] These structural relationships are most recently upheld by single-crystal X-ray[9-11] and EXAFS results[12] on the FeMo proteins of nitrogenase. Given these similarities, we have utilized clusters with M = V, Mo and other heterometals to examine the effect of heterometal on redox potentials and core electron distribution[7] as a possible means of anticipating corresponding effects in the cofactors.

Other types of heterometal–iron–sulfur (M–Fe–S) clusters include the Mo- and W-capped prismanes and rhombic dodecahedra containing the cores $[M_2Fe_6(\mu_3\text{-}S)_6]$[13] and $[Ni_5Fe_3(\mu_4\text{-}S)_6]$,[14] respectively, and a species with the cubane-type $[FeMo_3(\mu_3\text{-}S)_4]$ core.[15] At present, these structures while of some general interest do not enjoy established biological relevance. In recent research on new routes to M–Fe–S clusters, we found that the assembly systems $MCl_3(THF)_3$/$FeCl_2(PEt_3)_2$/$(Me_3Si)_2S$ in THF afforded in fair yield the clusters $MFe_4S_6(PEt_3)_4Cl$ with M = V and Mo.[16] These two clusters have the same overall C_{3v} structure, which is depicted in Figure 1. The structure consists of a cuboidal $[Fe_4S_3]$ cluster with the bottom iron atom in a tetrahedral site and the three symmetry-related iron atoms in the type of trigonal pyramidal coordination arrangement found in the clusters $Fe_6S_6(PEt_3)_6L_2$ (L = halide,[17] RS^- [18]) and $Fe_7S_6(PEt_3)_4Cl_3$.[19] These three iron atoms are each bridged by a μ_2-S atom to the heterometal M, which itself is encountered in trigonal pyramidal coordination. To our knowledge, this stereochemistry has not been previously observed in vanadium or molybdenum compounds.

The structures of $MFe_4S_6(PEt_3)_4Cl$, which because of their unusual features are of considerable interest in their own right,

⊗ Abstract published in *Advance ACS Abstracts,* November 1, 1994.

(1) Damon Runyon-Walter Winchell Cancer Research Fund Fellow, DRG-1206, 1992–1994.
(2) Holm, R. H.; Simhon, E. D. In *Molybdenum Enzymes*; Spiro, T. G., Ed.; Wiley-Interscience: New York, 1985; Chapter 1.
(3) Coucouvanis, D. *Acc. Chem. Res.* **1991**, *24*, 1.
(4) Holm, R. H. *Adv. Inorg. Chem.* **1992**, *38*, 1.
(5) Ciurli, S.; Ross, P. K.; Scott, M. J.; Yu, S.-B.; Holm, R. H. *J. Am. Chem. Soc.* **1992**, *114*, 5415.
(6) Zhou, J.; Scott, M. J.; Hu, Z.; Peng, G.; Münck, E.; Holm, R. H. *J. Am. Chem. Soc.* **1992**, *114*, 10843.
(7) Cen, W.; Lee, S. C.; Li, J.; MacDonnell, F. M.; Holm, R. H. *J. Am. Chem. Soc.* **1993**, *115*, 9515.
(8) Burgess, B. K. *Chem. Rev.* **1990**, *90*, 1377.
(9) Kim, J.; Rees, D. C. *Science* **1992**, *257*, 1677.
(10) Chan, M. K.; Kim, J.; Rees, D. C. *Science* **1993**, *260*, 792.
(11) Kim, J.; Woo, D.; Rees, D. C. *Biochemistry* **1993**, *32*, 7104.
(12) Chen, J.; Christiansen, J.; Campobasso, N.; Bolin, J. T.; Tittsworth, R. C.; Hales, B. J.; Rehr, J. J.; Cramer, S. P. *Angew. Chem., Int. Ed. Engl.* **1993**, *32*, 1592.
(13) (a) Coucouvanis, D.; Salifoglou, A.; Kanatzidis, M. G.; Dunham, W. R.; Simopoulos, A.; Kostikas, A. *Inorg. Chem.* **1988**, *27*, 4066. (b) Al-Ahmad, S. A.; Salifoglou, A.; Kanatzidis, M. G.; Dunham, W. R.; Coucouvanis, D. *Inorg. Chem.* **1990**, *29*, 927. (c) Chen, J.; Christiansen, J.; Tittsworth, R. C.; Hales, B. J.; George, S. J.; Coucouvanis, D.; Cramer, S. P. *J. Am. Chem. Soc.* **1993**, *115*, 5509.
(14) Saak, W.; Pohl, S. *Angew. Chem., Int. Ed. Engl.* **1991**, *30*, 881.
(15) (a) Shibahara, T.; Akashi, H.; Kuroya, H. *J. Am. Chem. Soc.* **1986**, *108*, 1342. (b) Dimmock, P. W.; Sykes, A. G. *J. Chem. Soc., Dalton Trans.* **1990**, 3101.
(16) Nordlander, E.; Lee, S. C.; Cen, W.; Wu, Z. Y.; Natoli, C. R.; Di Cicco, A.; Filipponi, A.; Hedman, B.; Hodgson, K. O.; Holm, R. H. *J. Am. Chem. Soc.* **1993**, *115*, 5549.
(17) Snyder, B. S.; Holm, R. H. *Inorg. Chem.* **1988**, *27*, 2339.
(18) Reynolds, M. S.; Holm, R. H. *Inorg. Chem.* **1988**, *27*, 4494.
(19) Noda, I.; Snyder, B. S.; Holm, R. H. *Inorg. Chem.* **1986**, *25*, 3851.

0020-1669/94/1333-5809$04.50/0

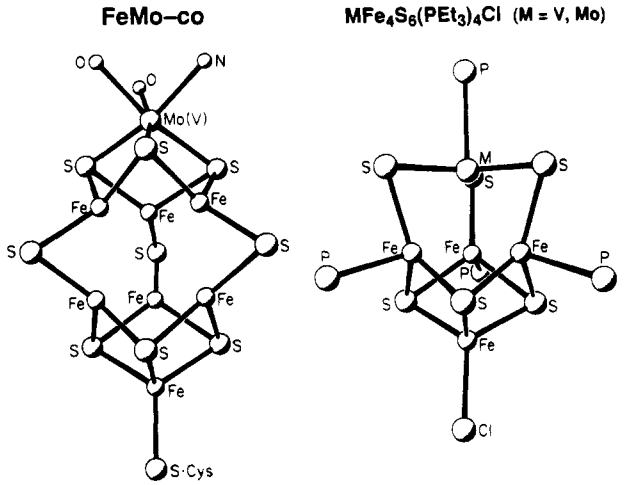

Figure 1. Comparison of the structures of the FeMo-cofactor of nitrogenase as found in MoFe proteins[9-11] and the synthetic clusters $MFe_4S_6(PEt_3)_4Cl$ (M = V, Mo),[16] conveying the presence of the common fragment $Fe_4(\mu_3\text{-}S)_3(\mu_3\text{-}S)_3$.

assume additional significance when compared with the structure of the FeMo-cofactor of nitrogenase determined by protein crystallography.[9-11] These structures are compared in Figure 1, from which it is evident that the 10-atom $[Fe_4(\mu_3\text{-}S)_3(\mu_2\text{-}S)_3]$ portion of $MFe_4S_6(PEt_3)_4Cl$ is contained in the FeMo-cofactor with the same bond connectivity and similar spatial arrangement. The cofactor, whose depiction is produced from protein coordinates, consists of cuboidal $[MoFe_3S_3]$ and $[Fe_4S_3]$ units bridged by three μ_2-S atoms to form a 17-atom core of idealized trigonal symmetry. Cuboidal $[Fe_4S_3]$ is an uncommon structural fragment, being otherwise established only in Roussin's black anion $[Fe_4S_3(NO)_7]^{1-}$ [20] and in $[Fe_4S_3(NO)_4(PPh_3)_3]^{0,1+}$.[21] The mean Fe−S and short Fe−Fe distances of 2.27−2.29 and 2.62 Å, respectively, have been determined by EXAFS analysis of the cofactor.[12] The corresponding distances in $MoFe_4S_6(PEt_3)_4Cl$ are 2.25 and 2.71 Å.[16] Because of these structural similarities, the $MFe_4S_6(PEt_3)_4Cl$ clusters are plausible precursors to higher nuclearity species that might more closely approach the bridged double-cuboidal stereochemistry of the cofactor. However, clarification of certain reactivity and electronic properties of these clusters is desirable prior to synthesis experiments. These include substitution reactions at iron sites, structures of substituted clusters, ground state spins, charge distribution and oxidation states, and the existence of other cluster oxidation states. These matters are addressed in this report.

Experimental Section

Preparation of Compounds. All operations were performed under a pure dinitrogen atmosphere with use of standard Schlenk and glove box techniques. Solvents were dried and degassed prior to use. The preparations of compounds **1** and **2** are simpler and afford equal or better yields (based on Fe) than those reported previously.[16] ^1H NMR and mass spectra of these compounds have been presented.[16] Yields in the following preparations are based on $FeCl_2(PEt_3)_2$.

$VFe_4S_6(PEt_3)_4Cl$ (1). A solution of 2.20 g (5.89 mmol) of $VCl_3(THF)_3$[22] in 80 mL of THF in a 200 mL Schlenk flask was heated to 50 °C, and was treated with 5.60 mL (26.5 mmol) of $(Me_3Si)_2S$. The reaction mixture was stirred and its color changed from orange to dark purple over 5 min. A solution of 4.40 g (12.1 mmol) of $FeCl_2(PEt_3)_2$[17] in 100 mL of THF was added dropwise to the reaction mixture maintained at 50 °C; an immediate color change to black ensued. The mixture was allowed to cool to room temperature and was stirred for 5 h. The dinitrogen atmosphere was removed by evacuation, a balloon containing 800 mL of air was connected to the reaction flask, and the mixture was stirred overnight under a closed aerobic atmosphere. During this period, ^1H NMR spectra of small aliquots of the reaction mixture taken to dryness and redissolved in $CDCl_3$ revealed increased formation of the desired cluster relative to the $Fe_6S_6(PEt_3)_4Cl_2$ byproduct, easily recognized by its equally intense signals at δ −6.59 and −7.72.[17] The final spectrum indicated the absence of this species. At this stage the reaction mixture consisted of a deep brown supernatant and a black precipitate. The supernatant liquid was removed from the solid by filtration and the solvent was removed in vacuo. The solid residue was washed with hexane and cold ether and was extracted with 5:1 ether/acetonitrile (v/v). The extract was filtered. Solvents were allowed to evaporate slowly until incipient crystallization. The mixture was cooled to −20 °C over 1 h and solvent evaporation was continued, resulting in the separation of the crystalline product. The procedure was terminated at the first appearance of white fiber-like crystals of byproducts (Et_3PS, Et_3PO). The supernatant was removed from the crystalline solid, which was washed with 10 mL of cold hexane and dried in vacuo. Multiple preparations each afforded 1.5−2.0 g (52−69%) of product as black crystals. Anal. Calcd for $C_{24}H_{60}ClFe_4P_4S_6V$: C, 29.57; H, 6.20; Cl, 3.64; Fe, 22.92; P, 12.71; S, 19.73; V, 5.23. Found: C, 30.79; H, 6.60; Cl, 3.35; Fe, 22.55; P, 12.55; S, 19.45; V, 4.74.

$MoFe_4S_6(PEt_3)_4Cl$ (2). The procedure is analogous to that for **1**. A solution of 1.40 g (3.34 mmol) of $MoCl_3(THF)_3$[23] in 80 mL of THF in a 200 mL Schlenk flask was heated to 50 °C and was treated with 3.00 mL (14.2 mmol) of $(Me_3Si)_2S$. The reaction mixture was stirred and its color changed from orange to dark purple over 10 min. A solution of 2.43 g (6.70 mmol) of $FeCl_2(PEt_3)_2$ in 50 mL of THF was added dropwise over 2 min, resulting in an immediate color change to black. Air (80 mL) was injected into the flask and the reaction mixture was stirred for 4 h. The ^1H NMR spectrum of a small aliquot revealed the major product to be **2**. The solvent was removed in vacuo, the residue was washed with 2 × 50 mL of hexanes and was dissolved in 100 mL of 5:1 ether/acetonitrile (v/v). The solution was cooled to 0 °C and was filtered. Slow evaporation of the filtrate followed by cooling to −20 °C afforded 0.70 g (41%) of product as black crystals. Anal. Calcd for $C_{24}H_{60}ClFe_4MoP_4S_6$: C, 28.27; H, 5.93; Cl, 3.48; Fe, 21.91; Mo, 9.41; P, 12.15; S, 18.86. Found: C, 28.36; H, 5.88; Cl, 3.55; Fe, 21.80; Mo, 9.27; P, 12.28; S, 18.75.

$VFe_4S_6(PEt_3)_4(SPh)$ (3). A 200 mL Schlenk flask was charged with 0.300 g (0.309 mmol) of **1** and 0.069 g (0.525 mmol) of NaSPh. The flask was connected to a solvent trap and 60 mL of 1:1 THF/acetonitrile (v/v) was added. The mixture was vigorously stirred and solvent removal in vacuo was initiated. A dry black solid residue was obtained within 20 min. The residue was extracted with 200 mL of hexane, and the solution was filtered. Slow concentration of the solution caused precipitation of the product, which was obtained as 0.262 g (81%) of a highly crystalline black solid. ^1H NMR (C_6D_6): δ 8.82 (*o*-H), 7.80 (*p*-H), 6.60 (*m*-H), 2.31 ($VPCH_2$), 1.39 ($VPCH_2CH_3$), 0.72 ($FePCH_2CH_3$), −1.05 ($FePCH_2$). FAB-MS (3-nitrobenzyl alcohol): *m/e* 1049 (M^+). Anal. Calcd for $C_{30}H_{65}Fe_4P_4S_7V$: C, 34.37; H, 6.25; Fe, 21.31; P, 11.82; S, 21.41; V, 4.86. Found: C, 34.51; H, 6.34; Fe, 21.24; P, 11.72; S, 21.49; V, 4.78.

$MoFe_4S_6(PEt_3)_4(SPh)$ (4). A procedure analogous to that for **3** was followed, utilizing 0.200 g (0.196 mmol) of **2** and 0.040 g (0.303 mmol) of NaSPh. The reaction was allowed to proceed for 30 min; the reaction mixture was rapidly taken to dryness, leaving a black powdery residue. This material was extracted with 150 mL of hexane and the extract was filtered. The filtrate was slowly reduced in volume, resulting in the isolation of the pure product as 0.190 g (88%) of black crystalline solid. ^1H NMR (C_6D_6): δ 12.90 (*o*-H), 11.80 (*p*-H), 4.26 (*m*-H), 1.21 ($MoPCH_2CH_3$), 0.77 ($FePCH_2CH_3$), −0.96 ($MoPCH_2$), −2.56 ($FePCH_2$). FAB-MS (3-nitrobenzyl alcohol): *m/e* 1095 (M^+). Anal. Calcd for $C_{30}H_{65}Fe_4MoP_4S_7$: C, 32.96; H, 5.99; Fe, 20.43; Mo, 8.77; P, 11.33; S, 20.53. Found: C, 33.05; H, 5.90; Fe, 20.29; Mo, 8.61; P, 11.42; S, 20.46.

(20) (a) Chu, C. T.-W.; Dahl, L. F.; *Inorg. Chem.* **1977**, *16*, 3245. (b) Glidewell, C.; Lambert, R. J.; Harman, M. E.; Hursthouse, M. B. *J. Chem. Soc., Dalton Trans.* **1990**, 2685.
(21) Scott, M. J.; Holm, R. H. *Angew. Chem., Int. Ed. Engl.* **1993**, *32*, 564.
(22) Manzer, L. E. *Inorg. Synth.* **1982**, *21*, 138.
(23) Dilworth, J. R.; Zubieta, J. *Inorg. Synth.* **1986**, *24*, 193.

$VFe_4S_6(PEt_3)_4(SEt)$ (5). A procedure analogous to that for **3** was followed, utilizing 0.200 g (0.206 mmol) of **1**, 0.030 g (0.36 mmol) of NaSEt, and 40 mL of the mixed solvent in a 100 mL flask. Solvent removal was completed within 15 min. The residue was extracted with 100 mL of hexane and the extract was filtered. Slow concentration of the filtrate afforded 0.128 g (62%) of product as a black crystalline solid. This compound was identified by spectroscopy and microprobe analysis. ^1H NMR (C_6D_6): δ 2.34 ($VPCH_2$), 1.46 ($VPCH_2CH_3$), 0.61 ($FePCH_2CH_3$), 0.55 ($FeSCH_2CH_3$), −2.09 ($FePCH_2$), −11.21 ($FeSCH_2$). FAB-MS (3-nitrobenzyl alcohol): *m/e* 939 $(M - SEt)^+$, 821 $(M - SEt - PEt_3)^+$, 703 $(M - SEt - 2PEt_3)^+$, 584 $(M - SEt - 3PEt_3)^+$. Atom ratio: Fe:V = 3.8:1 (microprobe analysis).

$MoFe_4S_6(PEt_3)_4(SEt)$ (6). A procedure analogous to that for **3** was followed, utilizing 0.100 g (0.098 mmol) of **1**, 0.015 g (0.179 mmol) of NaSEt, and 30 mL of mixed solvent in a 100 mL flask. After solvent addition, the mixture was vigorously stirred forming a brown slurry within 2 min. At this point, solvent removal was initiated and was completed after 20 min, leaving a black solid residue. Slow concentration of the filtrate from extraction with 100 mL of hexane afforded 0.064 g (62%) of product as a black crystalline solid. ^1H NMR (C_6D_6): δ 1.20 ($MoPCH_2CH_3$), 0.89 ($FePCH_2CH_3$), −1.95 ($MoPCH_2$), −2.12 ($FeSCH_2CH_3$), −2.95 ($FePCH_2$), −51.3 ($FeSCH_2$). This compound is quite unstable even under anaerobic conditions; satisfactory analyses and mass spectrum were not obtained.

$MoFe_4S_6(PEt_3)_4(S\text{-}p\text{-}C_6H_4OMe)$ (7). This compound, which was utilized for structure comparison, was prepared by a procedure analogous to that for **3** and was identified by X-ray diffraction of a crystal grown from a concentrated acetone solution. Crystallographic data: triclinic, space group $P\bar{1}$, a = 10.540(3) Å, b = 12.526(4) Å, c = 20.653(4) Å, α = 104.57(2)°, β = 90.58(2)°, γ = 112.52(2)°, V = 2421(1) Å^3, Z = 2, T = 223 K. The structure was solved as for **4** (vide infra). A total of 6353 unique reflections were refined to values of $R(R_w)$ = 5.88(4.13)%.

Collection and Reduction of X-ray Data. Black crystals of **3** and **4** were grown by slowly cooling concentrated solutions in ether/hexane and acetone, respectively. Single crystals were coated with Paratone-N oil and attached to glass fibers. The crystals were then transferred to a Nicolet R3mv diffractometer and cooled with a nitrogen stream. Lattice parameters of both compounds were obtained from a least-squares analysis of carefully centered reflections with $10° \le 2\theta \le 30°$. Decay corrections were based on the measured intensities of three reflections monitored periodically throughout the course of the data collections; neither compound showed significant decay. The raw intensity data were converted to structure factor amplitudes and their esd's by correction for scan speed, background, and Lorentz and polarization effects using the program XDISK of the SHELXTL PLUS program package. Empirical absorption corrections based on the observed variation in intensity of azimuthal scans (Ψ-scans) were applied to both data sets using the program XEMP. Compound **3** crystallized in a triclinic system. The space group was assigned as $P\bar{1}$ by statistics as well as by the successful refinement of the structure. Compound **4** crystallized in a monoclinic system; the systematic absences ($0k0$, $k = 2n + 1$; $h0l$, $h + l = 2n + 1$) identified the space group as $P2_1/n$. Crystallographic data are contained in Table 1.

Structure Solution and Refinement. Both structures were solved by direct methods and were refined via standard least-squares and Fourier techniques. All non-hydrogen atoms of **3** were refined with anisotropic thermal parameters. Owing to the limited amount of observed data, all carbon atoms in **4** were refined isotropically. Hydrogen atoms were assigned idealized locations and were given a uniform value of B_{iso}. The asymmetric unit of **3** consists of one complete cluster while that of **4** consists of two complete cluster molecules. The phosphine ligands in all of the clusters showed pronounced thermal motion. One of the phosphine methyl groups in **4** was disordered over two positions and was refined with each position having a 0.5 occupancy factor. In the last cycles of refinement, all parameters shifted by <1% of the esd of the parameter, and final difference Fourier maps showed no significant electron density. Final R factors are included in Table 1.[24]

(24) See paragraph at the end of this article concerning supplementary material.

Table 1. Crystallographic Data[a] for $[MFe_4S_6(PEt_3)_4(SPh)]$, M = V (**3**), Mo (**4**)

	3	**4**
formula	$C_{30}H_{65}Fe_4P_4S_7V$	$C_{30}H_{65}Fe_4MoP_4S_7$
fw	1048.5	1093.5
crystal system	triclinic	monoclinic
a, Å	12.094(3)	20.796(6)
b, Å	13.651(3)	19.006(4)
c, Å	16.840(6)	26.076(7)
α, deg	112.19(2)	
β, deg	91.30(2)	108.64(2)
γ, deg	114.70(2)	
V, Å^3	2284(1)	9766(4)
space group	$P\bar{1}$	$P2_1/n$
Z	2	8
ϱ_{calcd}, g/cm^3	1.52	1.49
μ, mm^{-1}	1.92	1.86
R (R_w),[b,c] %	5.82 (5.37)	5.73 (6.11)

[a] T = 223 K; Mo Kα radiation (λ = 0.710 69 Å). [b] $R = \sum||F_o| - |F_c||/\sum|F_o|$. [c] $R_w = \{\sum[\omega(|F_o| - |F_c|)^2]/\sum[\omega|F_o|^2]\}^{1/2}$.

Other Physical Measurements. NMR, EPR, and Mössbauer spectroscopic measurements and electrochemical determinations were performed with the equipment and using the procedures described elsewhere.[7] Magnetic measurements were carried out at the Tufts Magnetometry Center using a SQUID magnetometer. Isomer shifts of ^{57}Fe are referenced to Fe metal at 298 K; redox potentials were measured at a Pt working electrode and are reported vs the SCE.

LIGAND SUBSTITUTION (M = V, Mo)

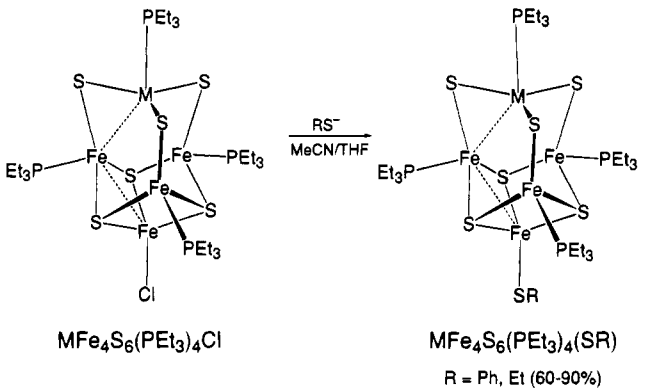

$MFe_4S_6(PEt_3)_4Cl$ $MFe_4S_6(PEt_3)_4(SR)$

R = Ph, Et (60-90%)

Figure 2. Schematic representation of the thiolate substitution reactions of $MFe_4S_6(PEt_3)_4Cl$ (M = V, Mo).

Results and Discussion

The following compounds are of principal interest in this investigation:

$VFe_4S_6(PEt_3)_4Cl$	**1**
$MoFe_4S_6(PEt_3)_4Cl$	**2**
$VFe_4S_6(PEt_3)_4(SPh)$	**3**
$MoFe_4S_6(PEt_3)_4(SPh)$	**4**
$VFe_4S_6(PEt_3)_4(SEt)$	**5**
$MoFe_4S_6(PEt_3)_4(SEt)$	**6**
$MoFe_4S_6(PEt_3)_4(S\text{-}p\text{-}C_6H_4OMe)$	**7**

Substitution Reactions. The unique Fe atoms in clusters **1** and **2** are designated as axial and the symmetry-related Fe atoms as equatorial. By means of the substitution reactions in Figure 2, thiolate-substituted clusters **3**−**6** have been prepared in the indicated yields. These reactions utilized *ca.* 50−80% excess NaSR and were conducted in relatively short times (15−30 min)

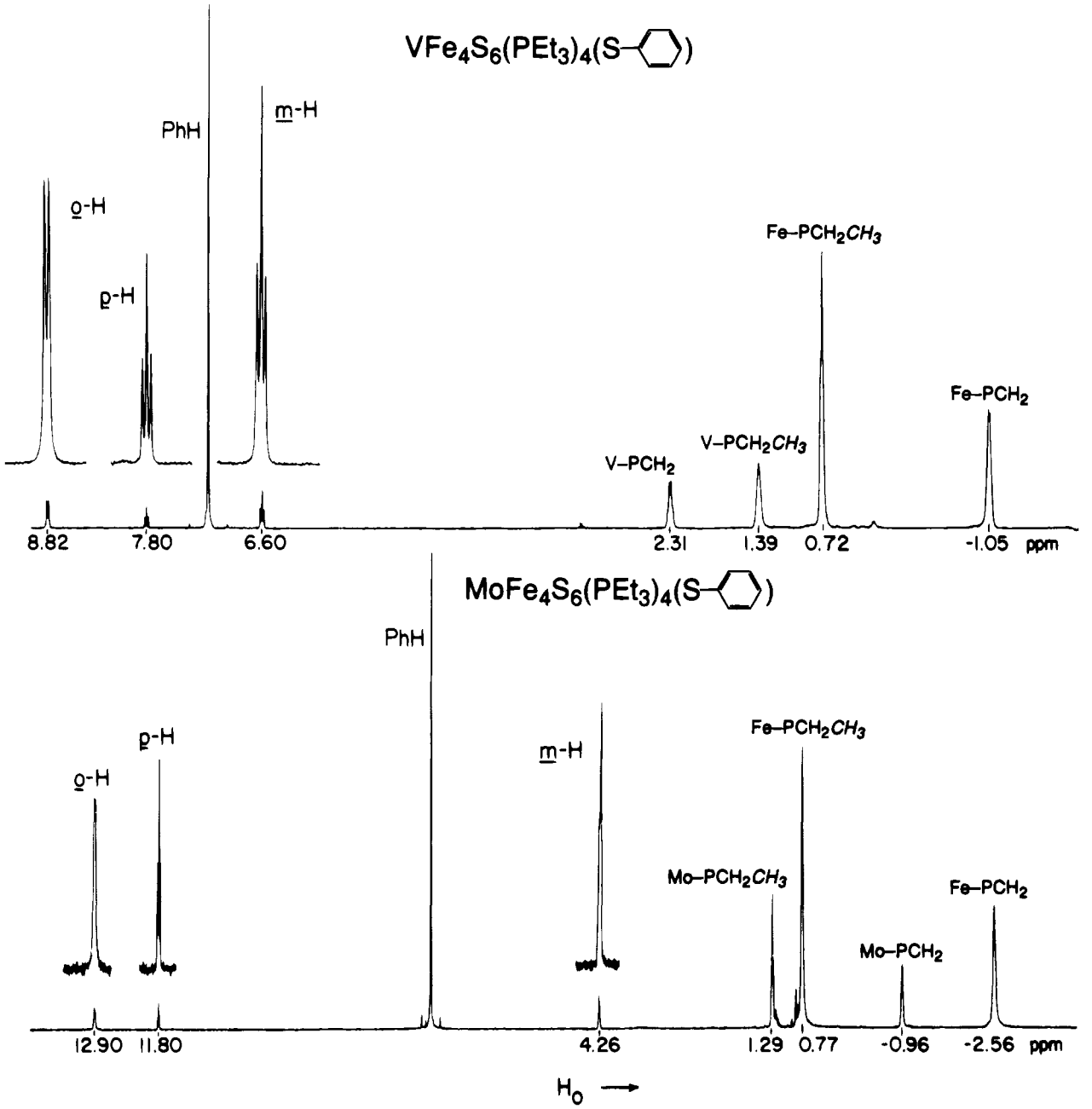

Figure 3. ^{1}H NMR spectra of $MFe_4S_6(PEt_3)_4(SPh)$ with M = V (upper) and Mo (lower) in C_6D_6 solutions. Signal assignments are indicated.

to avoid the formation of unidentified cluster byproducts. The ^{1}H NMR spectra of **3** and **4** are presented in Figure 3 and those of **5** and **6** are available in Figure 4. The four clusters give well-resolved, isotropically shifted spectra that are fully compatible with the retention of the core structures of **1/2** and substitution of chloride by thiolate. In this way, the expected lability of terminal chloride was found to be comparable with, e.g., that in the subsite-differentiated cluster $[Fe_4S_4(LS_3)Cl]^{2-}$,[25] and permitted a structural and electronic probe to be inserted at the axial Fe site. The thiolate substituent simulates cysteinate binding in the enzyme.[9-11]

Structures of Thiolate-Substituted Clusters. The structures of **3** and **4** are set out in Figure 5; metric parameters are provided in Table 2. Unlike **1** and **2**, which crystallize in trigonal space group *R*3*c* with imposed C_3 symmetry,[16] the two benzenethiolate clusters do not form isomorphous crystals nor are they subject to imposed symmetry. The cores of the clusters are preserved upon substitution with only minor dimensional changes between **1/2** and **3/4**. As in **1**, the vanadium atom in **3** is placed in the indicated trigonal pyramidal coordination site rather than at any cuboidal Fe site on the basis of the V−P(1) distance of 2.480(6) Å. All Fe−P distances in trigonal pyramidal FeS_3P coordination fall in the narrow range of 2.27−2.32 Å,[17,18,26,27] and Fe−SR distances in tetrahedral $FeS_3(SR)$ fragments of $[Fe_4S_4]$ cubane clusters do not exceed *ca.* 2.33 Å.[28-30] From the tabulated bond angles, it is readily seen that coordination at the equatorial Fe(2−4) sites is trigonal pyramidal whereas that

(25) (a) Stack, T. D. P.; Holm, R. H. *J. Am. Chem. Soc.* **1988**, *110*, 2484. (b) Weigel, J. A.; Holm, R. H. *J. Am. Chem. Soc.* **1991**, *113*, 4184.

(26) Snyder, B. S.; Holm, R. H. *Inorg. Chem.* **1990**, *29*, 274.

(27) Cai, J.-H.; Chen, C.-N.; Liu, Q.-T.; Zhuang, B.-T.; Kang, B.-S.; Lu, J.-X. *Jiegou Huaxue (J. Struct. Chem.)* **1989**, *8*, 220.

(28) Berg, J. M.; Holm, R. H. In *Metal Ions in Biology*; Spiro, T. G., Ed.; Interscience: New York, 1982; Vol. 4, Chapter 1.

(29) Carney, M. J.; Papaefthymiou, G. C.; Spartalian, K.; Frankel, R. B.; Holm, R. H. *J. Am. Chem. Soc.* **1988**, *110*, 6084 and references therein. The longest Fe−SR distances are found in the reduced clusters $[Fe_4S_4(SR)_4]^{3-}$.

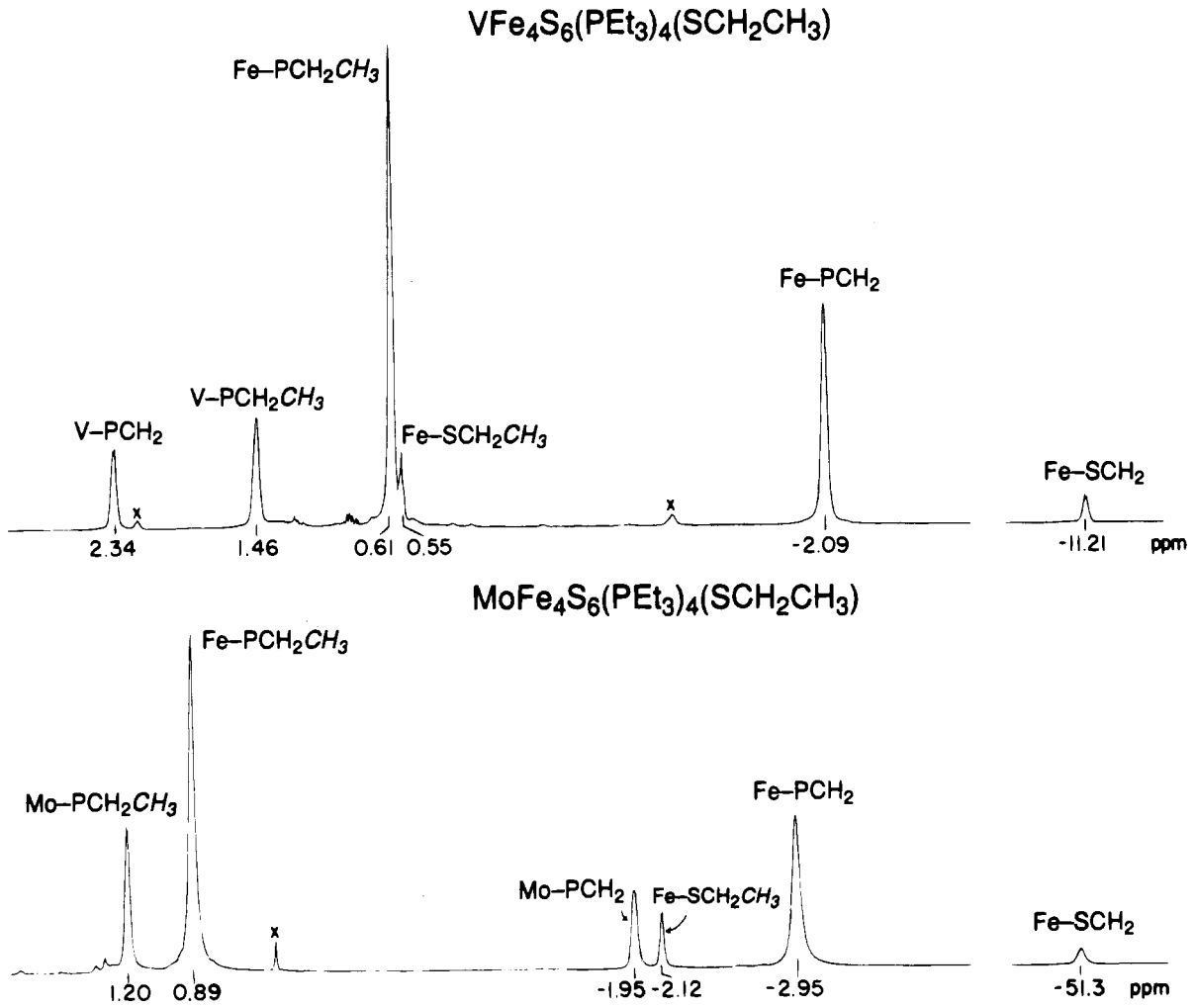

Figure 4. ^1H NMR spectra of $MFe_4S_6(PEt_3)_4(SEt)$ with M = V (upper) and Mo (lower) in C_6D_6 solutions. Signal assignments are indicated.

at the axial Fe(1) site is distorted tetrahedral. The mean core S–Fe–S angles at the axial site in **3** and **4** are both 103°; the corresponding values in $[Fe_4S_4(SPh)_4]^{2-,3-}$ are 104–105°,[30,31] respectively. The external angles S–Fe–SR are notoriously variable in cubane clusters, being dependent on lattice packing, and a similar behavior in **3** and **4** is thus not surprising. Because the structures of **1** and **2** are very similar to those of **3** and **4** and have been discussed previously,[16] we restrict attention to two structural features of the latter clusters that relate to electron distribution. Note that the molybdenum clusters have one more valence electron than the vanadium clusters.

Under idealized trigonal symmetry, there are five independent bonded distances within the Fe_4S_3 cuboidal fragment. In the labeling scheme of Figure 5, these are Fe(1)–S(2), Fe(2)–S(1), Fe(2)–S(2), Fe(1)–Fe(2), and Fe(2)–Fe(3). In molybdenum cluster **2**, every such distance is longer than the corresponding distance in vanadium cluster **1** by 0.044–0.071 Å. The effect extends to the Fe–P bond length, which is 0.031 Å longer in **2** than in **1**. In contrast, the Fe(2)–S(4) bridging distances, external to the fragment, are indistinguishable (2.240(2) Å in **2**, 2.234(1) Å in **1**).[16] In an assessment of **4** vs **3**, the same effect is found, and the number of independent distances is greater. Here the mean value of every cuboidal distance type in **4** and **7**, including Fe–P distances, is larger than the mean value in **3**. Further, practically all individual distance types in **4** and **7** are longer than the values in **3**. Again, the external bridging (mean) distances are practically the same (2.252(13) Å in **4**, 2.230(9) Å in **3**). While not all distance comparisons are statistically meaningful by a 3σ criterion, the trend is convincing. We interpret this to signify that the additional electron in **2** and **4** is antibonding and is largely confined to the Fe_4S_3 cuboidal fragment. That this is not a mechanical effect induced by the larger size of Mo vs V is supported by the relative insensitivity of bridging Fe–S distances external to and bonded angles within the cuboidal portion to variation in the heterometal. The metric effects observed here are analogous to those found in a comparison of $[Fe_4S_4(SR)_4]^{2-/3-}$ clusters.[28-31] The core Fe–S distances and volumes are always larger in the reduced core, for which theory places the additional electron in an antibonding core orbital of dominant iron character.[32]

Charge Distributions. (a) Bond Length Criteria. Terminal Fe–SR distances in the cubane-type $[Fe_4S_4(SR)_4]^{1-,2-,3-}$ clusters

(30) (a) Laskowski, E. J.; Frankel, R. B.; Gillum, W. O.; Papaefthymiou, G. C.; Renaud, J.; Ibers, J. A.; Holm, R. H. *J. Am. Chem. Soc.* **1978**, *100*, 532. (b) Stephan, D. W.; Papaethymiou, G. C.; Frankel, R. B.; Holm, R. H. *Inorg. Chem.* **1983**, *22*, 1550. (c) Carney, M. J.; Papaefthymiou, G. C.; Whitener, M. A.; Spartalian, K.; Frankel, R. B.; Holm, R. H. *Inorg. Chem.* **1988**, *27*, 346. (d) Carney, M. J.; Papaefthymiou, G. C.; Frankel, R. B.; Holm, R. H. *Inorg. Chem.* **1989**, *28*, 1497.

(31) (a) Que, L., Jr.; Bobrik, M. A.; Ibers, J. A.; Holm, R. H. *J. Am. Chem. Soc.* **1974**, *96*, 4168. (b) Excoffon, P.; Laugier, J.; Lamotte, B. *Inorg. Chem.* **1991**, *30*, 3075. The compound $(Bu_4N)_2[Fe_4S_4(SPh)_4]$ is reported to undergo a phase change at 243 K. The mean Fe–S bond length at 291 K (2.263(5) Å) is the same as that at 233 K (2.260 Å) but the difference in independent distances (2.238 Å, 2.281 Å) is larger.

(32) (a) Noodleman, L.; Norman, J. G., Jr.; Osborne, J. H.; Aizman, A.; Case, D. A. *J. Am. Chem. Soc.* **1985**, *107*, 3418. (b) Noodleman, L. *Inorg. Chem.* **1991**, *30*, 246.

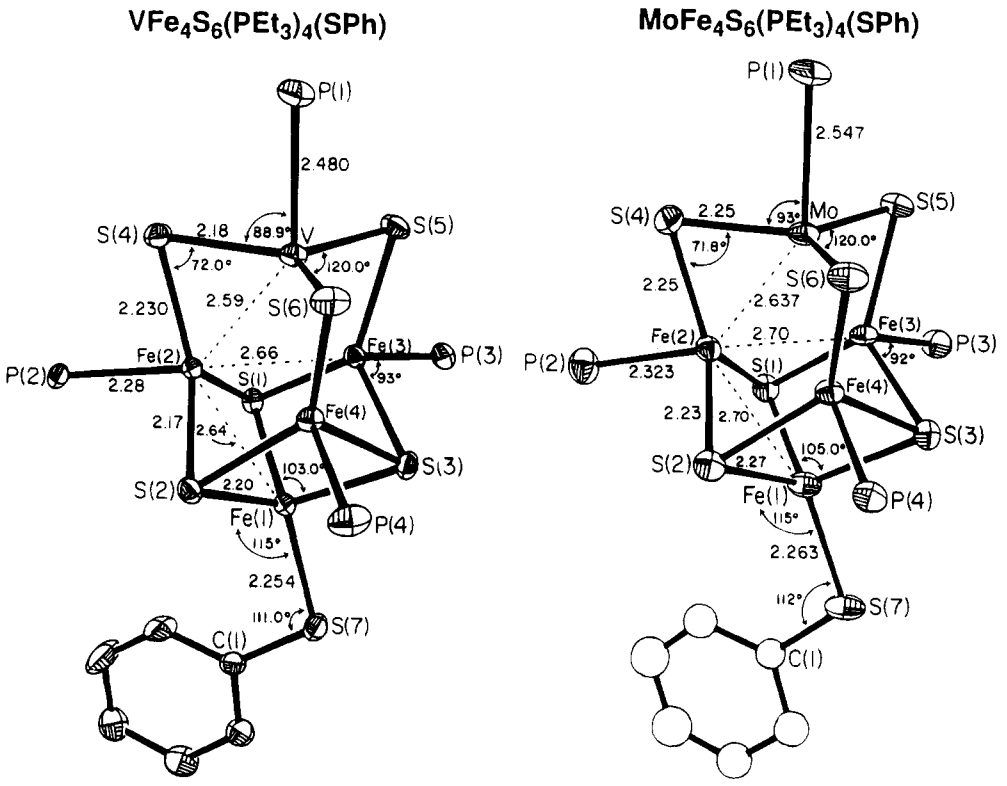

Figure 5. Structures of $MFe_4S_6(PEt_3)_4(SPh)$ (M = V, Mo) showing the atom labeling scheme, 50% probability ellipsoids, and selected mean values of interatomic distances and bond angles. One of the two crystallographically independent Mo clusters is depicted.

are well known to be sensitive to core oxidation state, becoming longer as the core oxidation level decreases in keeping with the larger radius of tetrahedral Fe(II) vs Fe(III).[28] Consequently, the axial Fe−L distances are a probe of the oxidation states of iron atoms in a tetrahedral FeS_3L environment, a situation most thoroughly developed for L = RS^-. The most appropriate available comparison of bond lengths in **3** and **4** is with the cubane clusters, whose distance dependence on oxidation state is summarized in Figure 6. The data are mean values or ranges of mean values for clusters with R = Ph (2−, 3−)[29−31] and R = 2,4,6-iPr$_3$C$_6$H$_2$ (1−).[33] Also included are data for $[Fe_4S_4Cl_4]^{2-}$;[34] this cluster type has been isolated in only one oxidation state. The Fe−Cl distances in **1** (2.227(2) Å) and **2** (2.263(4) Å) suggest that the axial iron atom in the former is slightly more oxidized than in the latter cluster. The Fe−SPh distances in **3** (2.254(5) Å) and **4** (2.263(9) Å), however, are indistinguishable. Both the core dimensions and axial bond length have been further investigated using the molybdenum cluster **7**. Like **3**, it crystallizes in triclinic space group $P\bar{1}$ facilitating a structural comparison less affected by crystal structure differences than with **3** and **4**. Its metric features are essentially identical with those of **4**; for this reason, they are not presented. The Fe−SPh bond length is 2.258(5) Å. Comparison of distance data is unlikely to be compromised[31b] by the difference in temperature between **1**−**4** (223 K) and the results in Figure 6 (*ca.* 300 K). By a bond length criterion (Figure 6), the data indicate that the effective oxidation state of the axial iron atom in **1**−**4** and **7** is, or is near, $Fe^{2.50+}$.

(b) ^{57}Fe Isomer Shifts. Isomer shifts (δ) and quadrupole splittings (ΔE_Q) for the vanadium [**1**,**3**,**5**] and molybdenum [**2**,**4**,**6**] cluster sets at 4.2 K are collected in Table 3. Spectra of the vanadium clusters, which are diamagnetic at 4.2 K, are illustrated in Figure 7. All spectra were analyzed at 4.2 and 100 K with a constrained 1:3 site population. Because of relaxation broadening, the spectrum of paramagnetic cluster **2** was poorly resolved at 4.2 K; data at 100 K are reported. Not all spectra could be uniquely analyzed. A procedure affording internally consistent parameters within the sets of vanadium or molybdenum clusters was followed. When statistically equivalent, the best fit was taken as that which gave consistent values for the equatorial iron sites, and axial site isomer shift differences Fe−Cl − Fe−SR ≈ 0.1 mm/s, as in $[Fe_4S_4]$ clusters.[35,36] The most appropriate comparisons of isomer shifts corresponding to known oxidation states are with synethetic and protein-bound Fe_4S_4 cubane clusters, protein-bound Fe_3S_4 cuboidal clusters, and certain synthetic clusters containing the cuboidal fragment.[37−42] In all cases, the iron atoms are in a tetrahedral FeS_3-

(33) O'Sullivan, T.; Millar, M. M. *J. Am. Chem. Soc.* **1985**, *107*, 4096.
(34) (a) Bobrik, M. A.; Hodgson, K. O.; Holm, R. H. *Inorg. Chem.* **1977**, *16*, 1851. (b) Müller, A.; Schladerberg, N. H.; Krickemeyer, E.; Bögge, H.; Schmitz, K.; Bill, E.; Trautwein, A. X. *Z. Anorg. Allg. Chem.* **1989**, *570*, 7. (c) Kawano, M.; Hoshino, C.; Sakai, K.; Matsumoto, K. *Anal. Sci.* **1991**, *7*, 829.
(35) Values of δ, ΔE_Q (mm/s): $(Et_4N)_2[Fe_4S_4(SEt)_2]$, 0.44, 1.21; $(Et_4N)_2[Fe_4S_4(SPh)_4]$, 0.47, 1.10; $(Ph_4P)_2[Fe_4S_4Cl_4]$, 0.51, 1.14.
(36) Alternative Mössbauer parameter sets δ, ΔE_Q (mm/s): **1**, 0.51, 1.23 (ax), 0.29, 1.53 (eq); **2**, 0.72, 0.65 (ax), 0.28, 1.06 (eq).
(37) Protein-bound $[Fe_3S_4]^{1+/0}$ clusters: (a) Huynh, B. H.; Moura, J. J. G.; Moura, I.; Kent, T. A.; LeGall, J.; Xavier, A. V.; Münck, E. *J. Biol. Chem.* **1980**, *255*, 3242. (b) Moura, J. J. G.; Moura, I.; Kent, T. A.; Lipscomb, J. D.; Huynh, B. H.; LeGall, J.; Xavier, A. V.; Münck, E. *J. Biol. Chem.* **1982**, *257*, 6259. (c) Kent, T. A.; Emptage, M. H.; Merkle, H.; Kennedy, M. C.; Beinert, H.; Münck, E. *J. Biol. Chem.* **1985**, *260*, 6871. (d) Surerus, K. K.; Kennedy, M. C.; Beinert, H.; Münck, E. *Proc. Natl. Acad. Sci. U.S.A.* **1989**, *86*, 9846.
(38) Synthetic $[Fe_3S_4]^0$ fragments: (a) Weigel, J. A.; Srivastava, K. K. P.; Day, E. P.; Münck, E.; Holm, R. H. *J. Am. Chem. Soc.* **1990**, *112*, 8015. (b) Coucouvanis, D.; Al-Ahmad, S. A.; Salifoglou, A.; Papaefthymiou, V.; Kostikas, A.; Simopoulos, A. *J. Am. Chem. Soc.* **1992**, *114*, 2472.
(39) Synthetic $[Fe_4S_4]^{3+}$ cluster: Papaefthymiou, V.; Millar, M. M.; Münck, E. *Inorg. Chem.* **1986**, *25*, 3010.
(40) Synthetic $[Fe_4S_4]^{2+}$ clusters: (a) Frankel, R. B.; Averill, B. A.; Holm, R. H. *J. Phys. (Paris)* **1974**, *35*, C6-107. (b) Kanatzidis, M. G.; Baenziger, N. C.; Coucouvanis, D.; Simopoulos, A.; Kostikas, A. *J. Am. Chem. Soc.* **1984**, *106*, 4500.

Table 2. Selected Interatomic Distances (Å) and Angles (deg) in $MFe_4S_6(PEt_3)_4(SPh)$ (M = V, Mo)

dist	M = V	M = Mo[a]	dist	M = V	M = Mo[a]
M−P(1)	2.480(6)	2.547(8)	Fe(1)−S(1)	2.192(4)	2.261(9)
M−S(4)	2.180(3)	2.226(10)	Fe(1)−S(2)	2.218(4)	2.275(10)
M−S(5)	2.203(5)	2.259(9)	Fe(1)−S(3)	2.204(3)	2.283(10)
M−S(6)	2.163(4)	2.254(9)	mean	2.20(1)	2.27(1)
mean	2.18(2)	2.25(2)			
			Fe(1)−Fe(2)	2.666(3)	2.762(6)
M−Fe(2)	2.611(3)	2.648(5)	Fe(1)−Fe(3)	2.620(3)	2.690(6)
M−Fe(3)	2.587(3)	2.646(5)	Fe(1)−Fe(4)	2.637(3)	2.662(5)
M−Fe(4)	2.581(4)	2.617(5)	mean	2.64(2)	2.70(5)
mean	2.59(2)	2.637(2)			
			Fe(2)−Fe(3)	2.684(3)	2.686(7)
Fe(2)−S(4)	2.239(5)	2.264(8)	Fe(2)−Fe(4)	2.612(2)	2.696(6)
Fe(3)−S(5)	2.221(5)	2.253(8)	Fe(3)−Fe(4)	2.671(3)	2.719(6)
Fe(4)−S(6)	2.229(5)	2.238(8)	mean	2.66(4)	2.70(2)
mean	2.230(9)	2.25(1)			
			Fe(2)−P(2)	2.293(3)	2.322(11)
Fe(2)−S(1)	2.183(4)	2.222(9)	Fe(3)−P(3)	2.284(4)	2.328(10)
Fe(2)−S(2)	2.173(5)	2.235(9)	Fe(4)−P(4)	2.257(4)	2.318(9)
Fe(3)−S(1)	2.181(3)	2.230(9)	mean	2.28(2)	2.323(5)
Fe(3)−S(3)	2.147(4)	2.214(9)			
Fe(4)−S(2)	2.188(4)	2.251(10)	Fe(1)−S(7)	2.254(5)	2.263(9)
Fe(4)−S(3)	2.174(4)	2.209(10)			
mean	2.17(1)	2.23(2)			

angle	M = V	M = Mo[a]	angle	M = V	M = Mo[a]
P(1)−M−S(4)	87.0(2)	90.6(3)	P(3)−Fe(3)−S(3)	95.7(1)	96.4(4)
P(1)−M−S(5)	90.1(2)	90.2(3)	P(3)−Fe(3)−S(5)	86.5(2)	91.8(3)
P(1)−M−S(6)	89.6(2)	87.8(3)	P(4)−Fe(4)−S(2)	95.3(2)	91.6(3)
			P(4)−Fe(4)−S(3)	96.3(1)	94.6(3)
S(4)−M−S(5)	122.2(2)	120.1(3)	P(4)−Fe(4)−S(6)	87.1(2)	89.8(3)
S(4)−M−S(6)	118.9(2)	119.6(4)			
S(5)−M−S(6)	118.8(1)	120.3(4)	S(1)−Fe(1)−S(2)	101.9(1)	100.1(4)
			S(1)−Fe(1)−S(3)	103.8(2)	103.4(3)
M−S(4)−Fe(2)	72.4(1)	72.3(3)	S(2)−Fe(1)−S(3)	103.4(1)	104.8(3)
M−S(5)−Fe(3)	71.6(2)	71.8(3)			
M−S(6)−Fe(4)	71.9(1)	71.2(3)	S(7)−Fe(1)−S(1)	120.2(2)	123.7(1)
			S(7)−Fe(1)−S(2)	122.4(2)	122.8(4)
P(2)−Fe(2)−S(1)	101.2(1)	92.6(4)	S(7)−Fe(1)−S(3)	102.4(1)	99.2(4)
P(2)−Fe(2)−S(2)	95.0(2)	96.8(4)			
P(2)−Fe(2)−S(4)	84.1(1)	88.3(4)	Fe(1)−S(7)−C(1)	111.0(5)	111.9(12)
P(3)−Fe(3)−S(1)	97.3(1)	89.5(3)			

[a] Data for one of the two inequivalent molecules in the asymmetric unit. Corresponding metric parameters in the two molecules are virtually identical.

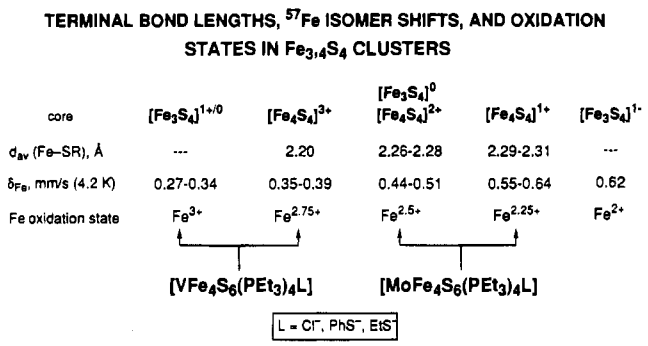

Figure 6. Relationship between Fe−SR bond lengths, ^{57}Fe isomer shifts, and (mean) oxidation states in cuboidal $[Fe_3S_4]$ and cubane-type $[Fe_4S_4]$ clusters. For $Fe^{2.5+}$, the limiting isomer shift of 0.51 mm/s is that of $[Fe_4S_4Cl_4]^{2-}$.[34]

(SR) coordination environment, but the group R, exact structure, and the medium of measurement are not necessarily constant. The isomer shifts in Figure 6 are ranges of values rather than averages; consequently, there is some overlap. However, for each oxidation state the large majority of clusters have isomer shifts in the middle of ranges.

Regardless of the parameter set selected,[36] the isomer shifts of the axial iron atoms in molybdenum clusters are larger than those in the vanadium clusters; i.e., the iron atoms are more

Table 3. Mössbauer Parameters for Cuboidal $MFe_4S_6(PEt_3)_4L$ Clusters at 4.2 K

cluster	site	δ, mm/s[a]	ΔE_Q, mm/s
$VFe_4S_6(PEt_3)_4Cl$	ax	0.40	1.01
	eq	0.28	1.53
toluene soln	ax	0.39	1.03
	eq	0.28	1.49
$VFe_4S_6(PEt_3)_4(SPh)$	ax	0.29	1.20
	eq	0.30	1.51
$VFe_4S_6(PEt_3)_4(SEt)$	ax	0.28	1.13
	eq	0.28	1.46
$MoFe_4S_6(PEt_3)_4Cl$[b]	ax	0.54	0.30
	eq	0.35	1.18
$MoFe_4S_6(PEt_3)_4(SPh)$	ax	0.48	0.76
	eq	0.32	1.00
$MoFe_4S_6(PEt_3)_4(SEt)$[c]	ax	0.46	0.54
	eq	0.37	1.41

[a] Relative to Fe metal at room temperature. [b] 100 K. [c] Broad lines (0.4−0.6 mm/s) because of incipient relaxation broadening.

(41) Synthetic $[Fe_4S_4]^{1+}$ clusters: Reference 30. Laskowski, E. J.; Reynolds, J. G.; Frankel, R. B.; Foner, S.; Papaefthymiou, G. C.; Holm, R. H. *J. Am. Chem. Soc.* **1979**, *101*, 6562.
(42) Protein-bound $[Fe_3S_4]^{1-}$ fragment: Surerus, K. K.; Münck, E.; Moura, I.; Moura, J. J. G.; LeGall, J. *J. Am. Chem. Soc.* **1987**, *109*, 3805.

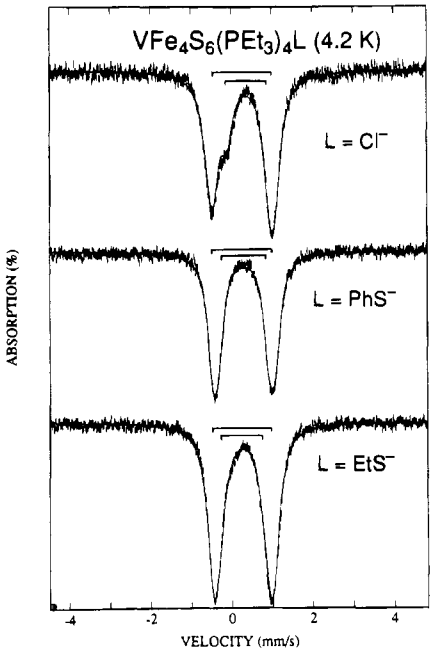

Figure 7. Mössbauer spectra of polycrystalline $VFe_4S_6(PEt_3)_4L$ (L = Cl^-, PhS^-, EtS^-) at 4.2 K.

reduced in the former. By an isomer shift criterion, the vanadium clusters possess axial iron atoms with oxidation states in the $Fe^{2.75+}$–Fe^{3+} range. In particular, the shifts of thiolate-ligated **3** and **5** are very close to those of the Fe^{3+} sites in $[Fe_3S_4]^{1+/0}$ proteins (0.27–0.32 mm/s). Application of the relationship between oxidation state s and isomer shift for tetrahedral $FeS_3(SR)$ units at 4.2 K,[7] $\delta = 1.36-0.36s$, affords $Fe^{2.97+}$ for **3** and $Fe^{3.00+}$ for **5**. Axial iron atoms in the molybdenum clusters fall in the $Fe^{2.5+}$–$Fe^{2.25+}$ interval, although the quadrupole splittings are smaller than might have been expected upon increasing the ferrous character of the cuboidal fragment.

Mössbauer parameters of equatorial iron sites are nearly constant within each cluster set, the iron atoms in the molybdenum set apparently being somewhat more reduced. Unfortunately, a relationship between isomer shift and oxidation state for trigonal pyramidal FeS_3P sites has yet to be established because of ambiguities in oxidation and spin states at such sites in the clusters $Fe_7S_6(PEt)_3Cl_3$, $Fe_6S_6(PEt_3)_4L_2$ (L = halide, PhS^-) and $[Fe_6S_6(PEt)_3]^{1+}$.[43] Together with **1**–**6**, these are the only Fe–S clusters known to contain trigonal pyramidal FeS_3P sites. This situation and the presence of heterometals prevent establishment of the equatorial iron oxidation states. We observe in passing, however, that the equatorial isomer shifts are similar to those of the spin-coupled all-Fe(III) cluster $[Fe_6S_8(PEt_3)_6]^{2+}$ (0.28 mm/s, 7 K),[44] and are in the regime of intermediate spin Fe(II,III) complexes[45] (but do not require these spin states). Noting also the trigonal d-orbital energy order $(xz, yz) < (x^2 - y^2, xy) < z^2$, the formulation $[V^{3+}(Fe_{eq}^{2+})_2Fe_{eq}^{3+}Fe_{ax}^{3+}]$ for [**1**,**3**,**5**] may be entertained. Here, $2Fe_{eq}^{2+}$ ($S = 1$) and Fe_{eq}^{3+} ($S = {}^3/_2$) are parallel-coupled to give $S = {}^7/_2$, which is then antiparallel-coupled with tetrahedral Fe_{ax}^{3+} ($S = {}^5/_2$) to yield cuboidal spin $S = 1$. When this is antiferromagnetically coupled to $S = 1$ of the d^2 heterometal, the observed $S = 0$ ground state is recovered. Similarly, the formulation $[Mo^{4+}(Fe_{eq}^{2+})_2Fe_{eq}^{3+}Fe_{ax}^{2+}]$ for [**2**,**4**,**6**] can lead to a $S = {}^1/_2$. These are not unique formulations in either spin or oxidation states, but are offered as initial considerations of complicated spin coupling problems, which are also posed by the Fe–S phosphine clusters[17–19,26,43] noted above. In any case, the axial iron isomer shift order $\delta_{Mo} > \delta_V$ is consistent with the cuboidal structural data.

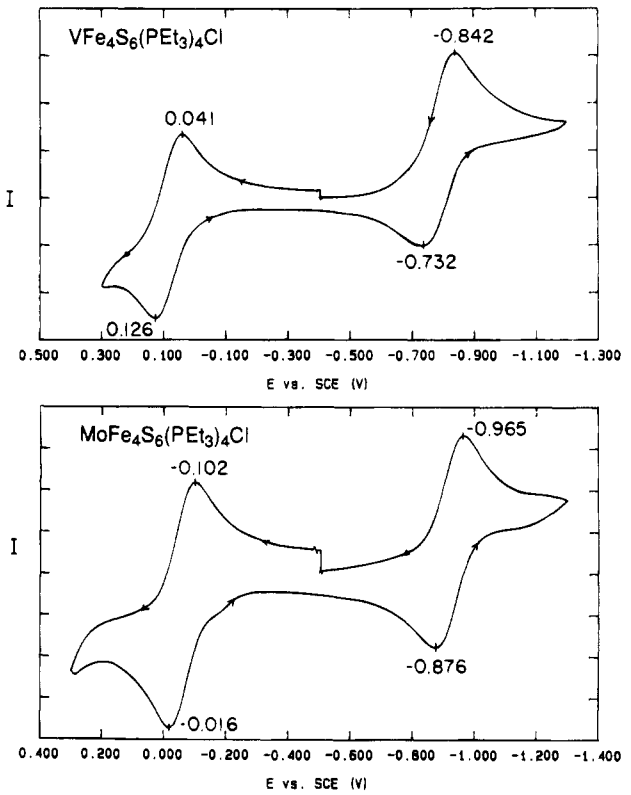

Figure 8. Cyclic voltammograms of $VFe_4S_6(PEt_3)_4Cl$ and $MoFe_4S_6(PEt_3)_4Cl$ in acetonitrile solutions at 298 K. Peak potentials vs SCE are indicated.

Table 4. Redox Potentials of $MFe_4S_6(PEt_3)_4L$ Clusters in Acetonitrile Solutions at 298 K

cluster	E_1,[a,b] V	E_2,[a,b] V
$VFe_4S_6(PEt_3)_4Cl$	+0.08	−0.79
$VFe_4S_6(PEt_3)_4(SPh)$	0.00	−0.86
$VFe_4S_6(PEt_3)_4(SEt)$	−0.05	−0.91
$MoFe_4S_6(PEt_3)_4Cl$	−0.06	−0.92
$MoFe_4S_6(PEt_3)_4(SPh)$	−0.16	−0.96
$MoFe_4S_6(PEt_3)_4(SEt)$	−0.20	−0.99

[a] $E_{1/2} = (E_{p,c} + E_{p,a})/2$; vs SCE; 100 mV/s, 0.1 M $(Bu_4N)(PF_6)$ supporting electrolyte. [b] $\Delta E_p = 81-100$ mV.

Electronic Transfer Properties. Clusters **1**–**6** exhibit two clean chemically reversible ($i_{pc}/i_{pa} \approx 1$) redox steps that define that three-membered electron transfer series (1).

$$[MFe_4S_6(PEt_3)_4L]^{1+} \overset{E_1}{\rightleftharpoons} [MFe_4S_6(PEt_3)_4L] \overset{E_2}{\rightleftharpoons} [MFe_4S_6(PEt_3)_4L]^{1-} \quad (1)$$

Typical cyclic voltammograms, for **1** and **2**, are shown in Figure 8 and potentials are compiled in Table 4. Certain regularities are immediately evident. For the steps E_1 and E_2 at parity of L, $E_V > E_{Mo}$ with $E_V - E_{Mo} = 140-160$ and 80–130 mV, respectively. The molybdenum clusters are more easily oxidized than the vanadium clusters. The same trend is observed in the two redox couples of M = V and Mo double cubanes

(43) Snyder, B. S.; Reynolds, M. S.; Holm, R. H.; Papaefthymiou, G. C.; Frankel, R. B. *Polyhedron* **1991**, *10*, 203. For comparison with the isomer shifts in this work, 0.12 mm/s must be subtracted from the published values.

(44) Del Giallo, F.; Pieralli, F.; Fiesoli, L.; Spina, G. *Phys. Lett.* **1983**, *96A*, 141.

(45) Greenwood, N. N.; Gibb, T. C. *Mössbauer Spectroscopy*; Chapman and Hall: London, 1971; Chapter 8.

Table 5. Selected Electronic Features of $[MFe_4S_6(PEt_3)_4L$ Clusters

cluster	property[a]
$VFe_4S_6(PEt_3)_4Cl$	$(\Delta H/H_0)_{iso}$: +3.63 ($FePCH_2$), +0.05 ($FePCH_2CH_3$); −1.17 ($VPCH_2$), −0.48 ($VPCH_2CH_3$) $S = 0/1$ equilibrium: $\Delta E = 192$ cm^{-1}, $g = 2.09$; $T_c = 282$ K, TIP $= 6.72 \times 10^{-5}$ emu/mol; $\mu_{eff} = 1.92\ \mu_B$ (300 K)
$VFe_4S_6(PEt_3)_4(SPh)$	$(\Delta H/H_0)_{iso}$: +2.31 ($FePCH_2$), +0.20 ($FePCH_2CH_3$); −1.05 ($VPCH_2$), −0.43 ($VPCH_2CH_3$); −0.96 (*o*-H), +0.66 (*m*-H), −0.66 (*p*-H)
$VFe_4S_6(PEt_3)_4(SEt)$	$(\Delta H/H_0)_{iso}$: +3.30 ($FePCH_2$), +0.30 ($FePCH_2CH_3$); −1.08 ($VPCH_2$), −0.49 ($VPCH_2CH_3$); +14.4 (SCH_2), +1.15 (SCH_2CH_3)
$MoFe_4S_6(PEt_3)_4Cl$	$(\Delta H/H_0)_{iso}$: +3.52 ($FePCH_2$), −0.08 ($FePCH_2CH_3$); +1.14 ($MoPCH_2$), −1.47 ($MoPCH_2CH_3$) $C = 0.659$ emu K/mol, $\theta = -2.03$ K, $\mu_{eff} = 2.00\ \mu_B$ (2.0−16 K); $\mu_{eff} = 2.95\ \mu_B$ (300 K); EPR: $g = 1.99$, 2.02, 2.15 (~10 K)[b]
$MoFe_4S_6(PEt_3)_4(SPh)$	$(\Delta H/H_0)_{iso}$: +3.68 ($FePCH_2$), +0.52 ($FEPCH_2CH_3$); +2.00 ($MoPCH_2$), −1.47 ($MoPCH_2CH_3$); −4.99 (*o*-H), +3.04 (*m*-H), −4.45 (*p*-H); $C = 0.542$ emu K/mol, $\theta = -1.47$ K, $\mu_{eff} = 2.00\ \mu_B$ (2.0−20 K); $\mu_{eff} = 2.74\ \mu_B$ (300 K)
$MoFe_4S_6(PEt_3)_4(SEt)$	$(\Delta H/H_0)_{iso}$: +4.04 ($FePCH_2$), +0.15 ($FePCH_2CH_3$); +2.99 ($MoPCH_2$), −0.49 ($MoPCH_2CH_3$); +54.1 (SHC_2), +3.79 (SCH_2CH_3)

[a] $(\Delta H/H_0)_{iso} = (\Delta H/H_0)_{dia} - (\Delta H/H_0)_{obs}$ (ppm, THF-d_8 solution); diamagnetic references are Et_3P, NaSEt, and NaSPh in THF. [b] 2-MeTHF.

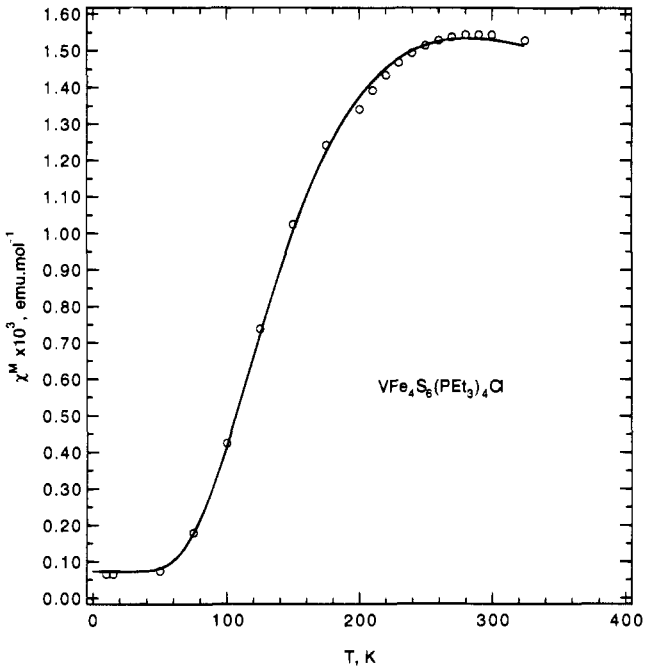

Figure 9. Temperature dependence of the magnetic susceptibility of $VFe_4S_6(PEt_3)_4Cl$ (4.2−300 K). Open circles are experimental points and the solid line is a fit to the data with the parameters in Table 5.

$[M_2Fe_6S_8(SEt)_9]^{3-/4-;4-/5-}$ but the potential difference is much larger (270−280 mV).[7] At parity of M in **1**−**6**, the ease of oxidation is $L = EtS^- > PhS^- > Cl^-$, the potential differences being 30−50 mV between the first and second substituents and 40−100 mV between the second and third substituents. The order of potentials is that expected on the basis of simple substituent effects and has been observed for the couples $[Fe_4S_4L_4]^{2-/3-}$ in DMF and acetonitrile solutions.[46] For the most part, the potential differences approximate one-fourth of those between $L = EtS^-/PhS^-$ and PhS^-/Cl^- couples (60−70 mV) of these cubane clusters. This result and the greater ease of oxidation of the molybdenum clusters are consistent with (but cannot be said to prove) redox processes largely localized in the Fe_4S_3 cuboidal portions of clusters **1**−**6**.

Electronic Features. Relevant NMR, EPR, and magnetic data are collected in Table 5. The magnetic behavior of vanadium cluster **1**, set out in Figure 9, is consistent with an $S = 0 \rightleftarrows S = 1$ spin equilibrium. The data could be fitted to the usual expression[47] with a singlet−triplet separation of 192 cm^{-1}. Attempted fits to an $S = 2$ excited state were unsatisfactory. While we have demonstrated the occurrence of physical mixtures of different spin states and spin-admixed ground states in $[Fe_4S_4(SR)_4]^{3-}$ clusters,[29] we have not before encountered a thermal equilibrium of spin states in any type of Fe−S cluster. Molybdenum clusters **2** and **4** have paramagnetic ground states that obey the Curie−Weiss law $\chi^M = C/(T - \theta)$ at low temperatures; Curie constants are in excess of that for an $S = {}^1/_2$ state ($C = 0.375$ for $g = 2$) but much less than that for an $S = {}^3/_2$ state ($C = 1.875$ for $g = 2$). These clusters may be cases of spin-admixed ground states with a minor $S = {}^3/_2$ component, at least in the solid state. At higher temperatures the susceptibilities of both clusters deviate from linearity in a manner consistent with occupation of excited state(s) of higher spin multiplicity. The EPR spectrum of **2** in frozen 2-MeTHF solution at low temperature is that of a rhombic $S = {}^1/_2$ species with $g_{av} = 2.05$.

All clusters afford well-resolved ^1H NMR spectra at room temperature. The isotropic shifts of the ethyl groups of the phosphine ligands at the Fe_{eq} and M sites are difficult to interpret because contact vs. dipolar contributions cannot be assessed at present. Isotropic shifts of thiolate substituents at the axial iron atoms are mainly contact in origin, based on alternating signs of phenyl proton shifts and ethyl group shift attenuations, by factors of 13 (**5**) and 14 (**6**) from methylene to methyl. The signs of the axial shifts are opposite to those of $[Fe_4S_4(SR)_4]^{2-,3-}$ clusters,[48] indicative of the placement of negative spin on the axial sulfur atoms which is delocalized consistent with contact interactions. This situation could occur if the three equatorial iron atoms are coupled to give a larger spin ($S = {}^7/_2$?) which is aligned parallel in an applied field and antiparallel-coupled to the lesser spin of $Fe_{ax}^{2+/3+}$ to afford the cuboidal fragment spin. The axial substituent shifts $|\Delta H/H_0|_{iso}$ in vanadium clusters **3** and **5** maximize at 276 K (compared to 282 K in solid **1**) and then decrease at higher temperatures, indicative of an equilibrium. However, we have been unable to fit the data satisfactorily to a singlet-triplet equilibrium[49] without invoking an unreasonably large temperature-independent additive term to the isotropic shifts. Clearly, the electronic structures of these clusters are complex. However, the ratio of axial substituent isotropic shifts, 3.3 (CH_3) and 3.8 (CH_2) in **6**/**5** and 4.6−6.7

(46) DePamphilis, B. V.; Averill, B. A.; Herskovitz, T.; Que, L., Jr.; Holm, R. H. *J. Am. Chem. Soc.* **1974**, *96*, 4159.

(47) $\chi^M = [2g^2\mu_B^2N/3kT][1 + (1/3)\exp(\Delta E/kT)]^{-1}$ + TIP, where ΔE is the singlet−triplet separation and the other symbols have their usual meaning: O'Connor, C. J. *Prog. Inorg. Chem.* **1982**, *29*, 203.

(48) Reynolds, J. G.; Laskowski, E. J.; Holm, R. H. *J. Am. Chem. Soc.* **1978**, *100*, 5315.

(49) (a) Holm, R. H. In *Dynamic Nuclear Magnetic Resonance*; Jackman, L. M., Cotton, F. A., Eds.; Academic Press: New York, 1975; Chapter 9. (b) Campbell, G. C.; Haw, J. F. *Inorg. Chem.* **1988**, *27*, 3706.

for the ring protons in **4/3**, is consistent with the ground states of the vanadium and molybdenum clusters and with the unpaired electron in the latter in the cuboidal fragment. The existence of this electron at the Mo site would not lead to such large differences in isotropic shifts of substituent groups located $\gtrsim 7$ Å from that site.

Summary

The following are the principal results and conclusions of this investigation.

(1) The chloride-ligated clusters **1** and **2** undergo facile ligand substitution reactions at the axial iron sites under carefully controlled conditions to afford the corresponding thiolate clusters **3**–**7** in isolated yields of *ca.* 60–80%. These clusters are readily recognized by their distinctive isotropically shifted ^{1}H NMR spectra. Thiolate groups serve as structural and electronic probes.

(2) The structures of thiolate clusters **3**, **4** and **7** demonstrate that the substitution reactions in (1) do not alter the $[Fe_4(\mu_3\text{-}S)_3(\mu_2\text{-}S)_3M]^{1+}$ core structure of precursors **1** and **2**. As previously observed,[16] the $Fe_4(\mu_3\text{-}S)_3(\mu_2\text{-}S)_3$ portion of this core is a structurally related major fragment of the core of the nitrogenase cofactor cluster.[9-11]

(3) There is a clear trend in corresponding bonded distances in the cuboidal Fe_4S_3 fragments such that those in the molybdenum clusters (**2**,**4**,**7**) are longer than those in the vanadium clusters (**1**,**3**).

(4) Axial Fe–S bond lengths approximate the oxidation state $Fe^{2.5+}$, and ^{57}Fe isomer shifts indicate the axial site oxidation state ranges $Fe^{2.75+}$–Fe^{3+} for the vanadium clusters and $Fe^{2.25+}$–$Fe^{2.5+}$ for the molybdenum clusters. Collective structural and Mössbauer and ^{1}H NMR spectroscopic results indicate that the additional valence electron in the molybdenum clusters is largely delocalized in the Fe_4S_3 cuboidal portion.

(5) Cluster **1** (and by inference **3** and **5**) exist in a singlet–triplet spin equilibrium, which is the first example of this behavior in any type of Fe–S cluster. Clusters **2** and **4** (and by inference **6**) have $S = {}^1/_2$ or spin-admixed $S = {}^1/_2, {}^3/_2$ ground states. Isotropic shifts of axial thiolate substituents in **3**–**6** are primarily contact in origin and are consistent with the ground states of vanadium and molybdenum clusters in the solid state.

This investigation together with prior work[43] makes evident the need to develop a spin-coupling model to account for the magnetic and NMR properties of homo- and heterometal iron–sulfur–phosphine clusters. We anticipate further investigations of these clusters pending the outcome of experiments in which $MFe_4S_6(PR_3)_4L$ species are utilized as precursors in synthetic elaborations toward higher-nuclearity clusters related to the nitrogenase cofactors. Such experiments are in progress.

Acknowledgment. This research was supported by NIH Grant GM 28856. X-ray diffraction equipment was obtained by NIH Grant 1 S10 RR 02247. We thank Dr. L. Cai for experimental assistance.

Supplementary Material Available: For the compounds in Table 1 and for compound **7**, tables of crystal and intensity collection data, positional and thermal parameters, and interatomic distances and angles (30 pages). This material is contained in many libraries on microfiche, and can be ordered from the ACS; see any current masthead page for ordering information.